UCLA
COMPUTATIONAL AND APPLIED MATHEMATICS

An Eulerian Approach for Vortex Motion Using a Level Set Regularization Procedure

Eduard Harabetian
Stanley Osher
Chi-Wang Shu

June 1995
(Revised October 1995)

CAM Report 95-30

Department of Mathematics
University of California, Los Angeles
Los Angeles, CA. 90024-1555

An Eulerian Approach for Vortex Motion Using a Level Set Regularization Procedure

Eduard Harabetian *
Department of Mathematics
University of Michigan
Ann Arbor, MI 48109

Stanley Osher †
Department of Mathematics
University of California
Los Angeles, CA 90024

Chi-Wang Shu ‡
Division of Applied Mathematics
Brown University
Providence, RI 02912

October 25, 1995

Key Words: Vortex motion, Eulerian, level sets, ENO scheme.
AMS (MOS) subject classification: 76C05, 76M20

*Research supported by NSF grant DMS-9204271 and AFOSR grant F49620-94-1-0215.
†Research supported by NSF grant DMS-9103104, ARO grant DAAL03-91-G-0162 and ARPA/ONR grant N00014-92-J-1890.
‡Research supported by ARO Grant DAAH04-94-G-0205, NSF Grant DMS-9500814, NASA Langley Grant NAG-1-1145 and AFOSR Grant 95-1-0074.

Abstract

We present an Eulerian, fixed grid, approach to solve the motion of an incompressible fluid, in two and three dimensions, in which the vorticity is concentrated on a lower dimensional set. Our approach uses a decomposition of the vorticity of the form $\xi = P(\varphi)\eta$, in which both φ (the level set function) and η (the vorticity strength vector) are smooth. We derive coupled equations for φ and η which give a regularization of the problem. The regularization is topological and is automatically accomplished through the use of numerical schemes whose viscosity shrinks to zero with grid size. There is no need for explicit filtering, even when singularities appear in the front. The method also has the advantage of automatically allowing topological changes such as merging of surfaces. Numerical examples including two and three dimensional vortex sheets, two dimensional vortex dipole sheets and point vortices, are given. To our knowledge, this is the first three dimensional vortex sheet calculation in which the sheet evolution feeds back to the calculation of the fluid velocity. Vortex in cell calculations for three dimensional vortex sheets were done earlier by Trygvasson et al in [16].

1 The General Formulation

We consider the motion of an incompressible fluid, in two and three dimensions, in which the vorticity is concentrated on a lower dimensional set. Prominent examples are vortex sheets and vortex filaments in three dimensions, and vortex sheets, vortex dipole sheets and point vortices in two dimensions [6],[7],[8],[9],[1],[2],[3],[17].

In three dimensions, the equations are written in the form

$$\begin{aligned} \xi_t + v\nabla\xi - \nabla v\ \xi &= 0 \\ \nabla \times v &= \xi \\ \nabla \cdot v &= 0 \end{aligned} \tag{1.1}$$

where $\xi(x,y,z,t)$ is the vorticity vector, and $v(x,y,z,t)$ is the velocity vector.

In a vortex sheet, ξ is a singular measure concentrated on a two dimensional surface, while in a vortex filament, ξ is a function concentrated on a tubular neighborhood of a curve.

Traditionally, these problems have been solved within a Lagrangian framework, in which the vorticity is carried along by fluid particles [6],[7],[8],[9],[2],[17]. Numerical methods based on this approach have the advantage that they adapt very well to the flow. On the other hand, they are not simple to implement in three dimensions and they may have difficulties with topological changes, such as merging of interfaces. Merging may occur for some of these problems (and certainly not for others such as the vortex patch problem). In addition, some kind of numerical filtering is needed to stabilize the resulting ill-posed system, especially when singularities appear in the front [6],[7],[8],[9].

In this paper we present an Eulerian, fixed grid, approach, that works in general in two and three dimensions. In the particular case of the two dimensional vortex sheet problem in which the vorticity does not change sign, the approach yields a very simple and elegant formulation.

The basic observation involves a variant of the level set method for capturing fronts, developed in [12], and found to have numerous applications in physics, engineering, differential geometry, computer vision, image processing and elsewhere – see e.g. [11],[15] and the references therein.

The present work grew out of a project [5] in which the first two authors regularized general ill-posed problems via the level set approach, using the idea that a simple

closed curve which is the level set of a function cannot change its index, i.e. there is an automatic topological regularization. This is very helpful for numerical calculations. The regularization is automatically accomplished through the use of dissipative schemes, which has the effect of adding a small curvature term (which vanishes as the grid size goes to zero) to the evolution of the interface. See [5] for more details. There is therefore no need for explicit filtering. This is typical of our approach to such ill-posed problems.

Our formulation allows for topological changes, such as merging of surfaces — see e.g. [15] where bubble merging is easily computed using similar ideas.

The main idea is to decompose ξ into a product of the form

$$\xi = P(\varphi)\eta \tag{1.2}$$

where P is a scalar function, typically an approximate δ function. The variable φ is a scalar function whose zero level set represents the points where vorticity concentrates, and η represents the vorticity strength vector. This decomposition is performed at time zero and is of course not unique.

Our observation is that once a decomposition is found, the following system of equations yields a solution to the Euler equations, replacing the original set of equations (1.1).

$$\begin{aligned} \varphi_t + v\nabla\varphi &= 0 \\ \eta_t + v\nabla\eta - \nabla v\ \eta &= 0 \\ \nabla \times v &= P(\varphi)\eta \\ \nabla \cdot v &= 0 \end{aligned} \tag{1.3}$$

These equations have initial conditions

$$\begin{aligned} \varphi(0,\cdot) &= \varphi_0 \\ \eta(0,\cdot) &= \eta_0 \end{aligned}$$

where φ_0, η_0 and P are chosen so that (1.2) holds at time $t = 0$. Notice that (1.2) and (1.3) imply that $\nabla\varphi$ is orthogonal to η, and $div(\eta) = 0$. This is enforced in the initial condition and is maintained automatically by (1.2) and (1.3).

The fact that smooth solutions of (1.2) and (1.3) satisfy the Euler equations can easily be verified by direct substitution of (1.2) into (1.1). Conversely, if there is a

unique solution to the initial-boundary value problem, (1.1), with appropriate boundary conditions, it will be computed through (1.2), (1.3).

When P is a distribution, such as a δ function, approaching P with a sequence of smooth mollifiers P_ϵ yields a sequence of approximating solutions. This is the approach used in numerical calculations, since the δ function can only be represented approximately on a finite grid. The parameter ϵ is usually chosen to be proportional to the mesh size.

The advantage of this formulation, is that it replaces a possibly singular and unbounded vorticity function ξ, by bounded, smooth (at least uniformly Lipschitz) functions φ and η. Therefore, while it is not feasible to compute solutions of (1.1) directly, it is very easy to compute solutions of (1.3).

When P_ϵ is a characteristic function, the approximate solution is a vortex patch. Bertozzi and Constantin [1] have previously used the idea of a level set function to present a simplified proof of Chemin's earlier results [3] concerning the regularity of the boundary of the patch for all time for two dimensional vortex patch problem.

The numerical method used in the next two sections, is the third order upwind biased ENO (Essentially Non-Oscillatory) scheme with a third order TVD Runge-Kutta time stepping [13, 4], coupled with a second order elliptic solver (FISHPAK) for the Poisson equations. The choice of ENO gives strong nonlinear stability: numerical viscosity is automatically adjusted according to the local smoothness of the solution, is maintained minimal by an adaptive stencil interpolation to automatically choose the locally smoothest region to gain information, and vanishes with grid size. It is our observation for these numerical tests that third order ENO gives very similar resolution to first order monotone schemes, with about half of the number of grid points in each direction, resulting in a factor of 16 reduction in the number of space-time grid points.

2 The 2D Equations and Examples

In two dimensions, the vorticity is given by

$$\xi = \begin{pmatrix} 0 \\ 0 \\ \omega(t,x,y) \end{pmatrix}$$

and hence the Euler equations are given by

$$\begin{aligned} \omega_t + v\nabla\omega &= 0 \\ curl(v) &= \omega \qquad (2.1) \\ div(v) &= 0 \qquad (2.2) \end{aligned}$$

Our formulation (1.3), becomes

$$\begin{aligned} \varphi_t + v\nabla\varphi = 0 \\ \eta_t + v\nabla\eta = 0 \qquad (2.3) \\ curl(v) = P(\varphi)\eta \\ div(v) = 0 \end{aligned}$$

where η is now a scalar.

If the vortex sheet strength η does not change sign along the curve, it can be normalized to $\eta \equiv 1$ and the equations take on a particularly simple and elegant form:

$$\varphi_t + v(\varphi)\nabla\varphi = 0 \qquad (2.4)$$

where the velocity $v(\varphi)$ is given by

$$v = -\begin{pmatrix} -\partial_y \\ \partial_x \end{pmatrix} \triangle^{-1} P(\varphi) \qquad (2.5)$$

In this case, the vortex sheet strength along the curve is given by $\frac{1}{|\nabla\varphi|}$ (see (3.1)).

Example 2.1 - Vortex Sheets in 2D. We consider the periodic vortex sheet in two dimensions, i.e. $P(\varphi) = \delta(\varphi)$ in (2.5). The three dimensional case is defined in detail in Example 3.1 of next section. The evolution of the vortex sheet in the Lagrangian framework has been considered by various authors. Krasny [6], [7] has computed vortex sheet roll-up using vortex blobs and point vortices with filtering. Baker and Shelley [2] have approximated the vortex sheet by a layer of constant vorticity which they computed by Lagrangian methods. In the context of our approach, their approximation corresponds to approximating the δ function by a step function.

In our framework, we use a fixed Eulerian grid, and approximate (2.4) by the third order upwind ENO finite difference scheme with a third order TVD Runge-Kutta time stepping [13, 4]. At every time step, the velocity v is first obtained by solving the Poisson equation for the stream function Ψ:

$$\Delta\Psi = -P(\varphi)$$

with boundary conditions

$$\Psi(x, \pm 1) = 0$$

and periodic in x. This is done by using a second order elliptic solver FISHPAK. Once Ψ is obtained, the velocity is recovered by $v = (-\Psi_y, \Psi_x)$ by using either ENO or central difference approximations (we do not observe major difference among the two: the results shown are those obtained by central difference). Once v is obtained, upwind biased ENO is easily applied to (2.4), [4].

The initial conditions are similar to the ones in [7], i.e given by a sinusoidal perturbation of a flat sheet:

$$\varphi_0(x, y) = y + 0.05 \sin(\pi x)$$

The boundary condition for φ are periodic, of the form:

$$\varphi(t, -1, y) = \varphi(t, 1, y)$$

$$\varphi(t, x, -1) = \varphi(t, x, 1) - 2$$

The δ function is approximated as in [14],[15] by

$$\delta_\epsilon(\phi) = \begin{cases} \frac{1}{2\epsilon}(1 + \cos\left(\frac{\pi\phi}{\epsilon}\right)) & \text{if } |\varphi| < \epsilon \\ 0 & \text{otherwise} \end{cases} \tag{2.6}$$

For fixed ϵ, there is convergence as $\Delta x \to 0$ to a smooth solution. One can then take $\epsilon \to 0$. This two step limit is very costly to implement numerically. Our numerical results show that one can take ϵ to be proportional to Δx, but convergence is difficult to establish theoretically.

In Figures 1(a) to 1(f), we present the result of using 128^2 grid points. The parameter ϵ in the approximate δ function is chosen as $\epsilon = 12\Delta x$. We use the graphic package TECPLOT to draw the level curve of $\varphi = 0$. Notice that this is restricted by the resolution of the contour procedure. The code can run in a stable way for much longer time, however the resolution at the core of roll-up will be gradually lost due to numerical errors. Next, we keep $\epsilon = 12\Delta x$ but double the grid points in each direction to 256^2, the result of $t = 4$ is shown in Figure 2(a). Comparing with Figure 1(e), we can see that there are more turns in the core at the same physical time when the grid size is reduced and the δ function width ϵ is kept proportional to Δx. One might wonder whether the core structure of Figure 2(a) is distorted by numerical error. To verify that this is not the case, we keep $\epsilon = 12 \times \frac{2}{256} = \frac{3}{32}$ *fixed*, and reduce Δx,

Figures 2(b) and 2(c). The three pictures overlay very well, Figures 2(b) and 2(c) are indistinguishable, indicating that the core structure is a resolved solution to the problem and convergence is obtained with fixed ϵ. By reducing ϵ for the more refined grids, more turns in the core can be obtained in shorter time (pictures not shown).

The smoothing of the δ function, and the third order truncation error in the advection step and the second order error in the inverse Laplacian are the only smoothing steps in our method.

Example 2.2 - Vortex Sheet Dipole. In this example, P is the derivative of the approximate δ function in (2.6), i.e.

$$P(\varphi) = \begin{cases} -\frac{\pi}{2\epsilon^2}\sin\left(\frac{\pi\varphi}{\epsilon}\right) & \text{if } |\varphi| < \epsilon \\ 0 & \text{otherwise} \end{cases} \tag{2.7}$$

The vorticity ω is chosen to be equal to $\alpha P(\varphi(x,y))$ where α is the amplitude of the dipole. From (2.7), we see that the vorticity is concentrated on two vortex sheets Γ_+, Γ_- which are of opposite sign and of distance ϵ apart, where $\Gamma_\pm$ are the level sets $\varphi = \pm\epsilon/2$. This example models the evolution of a very thin jet [8].

The equation (2.4) is again computed with the third order ENO scheme coupled with a second order potential solver, with the initial condition

$$\varphi_0(x,y) = \frac{y}{1 - 0.75\sin(\pi x)}$$

This represents a flat dipole sheet with a symmetric sinusoidal perturbation in strength.

The results of a grid with 256^2 points, at $t = 0$, 1, 2, 3, 4 and 5, are shown in Figures 3(a) to 3(f). We choose $\epsilon = 8\Delta x$ and the dipole amplitude $\alpha = 0.04$. In this computation, we set P equal to a different formula than (2.7):

$$P(\varphi) = \begin{cases} -\frac{1}{2\epsilon^2}\left(1 + \cos\left(\frac{\pi(\phi+\epsilon)}{\epsilon}\right)\right) & \text{if } -2\epsilon \le \varphi \le 0 \\ +\frac{1}{2\epsilon^2}\left(1 + \cos\left(\frac{\pi(\phi-\epsilon)}{\epsilon}\right)\right) & \text{if } 0 \le \varphi \le 2\epsilon \\ 0 & \text{otherwise} \end{cases}$$

We choose this formula because it allows one to control the dipole separation. In this case, we set the dipole separation equal to 2ϵ, i.e. Figures 3(a) to 3(f) show the level sets of $\varphi = \pm\epsilon$. The boundary conditions for the stream function Ψ and for φ are the same as in Example 2.1.

As the results show, the dipole sheet rolls up symmetrically, and the tips become more stretched with time until they "peel off" in Figure 3(f). This peel off is not

physical, and should be the result of lack of numerical resolution in the part of very thin and stretched tips of the bubble. To illustrate how much numerical errors are present in the figures, we also show in Figures 4(a) to 4(d) the results of 512^2 grid points, and in Figures 5(a) to 5(d) that of 1024^2 grid points, with the same $\epsilon = 8 \times \frac{2}{256}$, at $t = 2$, 3, 4 and 5. Comparing with Figures 3(c) and 3(f), we can see that the 256^2 results are basically resolved up to $t = 3$ but are slightly underresolved afterwards. However the structures of the solution between these different resolutions are still similar. Also notice that, in the most refined run in Figure 5, the "peel off" does not appear: the tip of the bubble is connected (this can be seen in a zoomed version of Figure 5(d)). These results are similar to the computations performed by Krasny [8].

Example 3 - Point Vortices. In this example, P is a δ function, and φ is supported at finite number of points in the plane: $x_1, x_2, ..., x_n$. For example, if the vorticity is positive, initially one may choose

$$\varphi_+(x) = \min_i \left(\frac{|x - x_i|}{a_i} \right)$$

where $a_i > 0$ are the vortex point strengths.

For point vortices with negative strength, one introduces a second level set function, φ_-. Both φ_+ and φ_- evolve by (2.4), where the velocity v is given by

$$v = - \begin{pmatrix} -\partial_y \\ \partial_x \end{pmatrix} \triangle^{-1} \left(\delta(\varphi_+) + \delta(\varphi_-) \right)$$

This procedure can be applied to a general n-body problem.

We will show the numerical result of three point vortices, two with positive strength $a_1 = 1$ and $a_2 = 2$, located at $x_1 = (-0.5, -0.5)$ and $x_2 = (-0.5, 0.5)$, respectively, and one with negative strength $a_3 = -3$ located at at $x_3 = (0.5, 0)$. The boundary condition for the stream function is $\Psi = 0$ at all four boundaries $x = \pm 1$ and $y = \pm 1$, and the boundary condition for φ is Neumann. We again use 256^2 grid points and $\epsilon = 12\Delta x$. The results at $t = 0$, 5, 10 and 15 are shown in Figures 6(a) to 6(d), where 10 contours from $\varphi = 0$ to $\varphi = 0.04$ are drawn, with the solid lines corresponding to the positive vortices φ_+ and dashed lines corresponding to the negative vortices φ_-.

The vortex patch problem is easier to compute as the function $P(\varphi)$ is less singular, and the results are omitted.

3 The 3D Equations and Examples

We now give two examples in three dimensions. Numerical results for the first example are also shown.

Example 3.1 - Vortex Sheets in 3D. In this example we sketch the algorithm for initializing and computing a periodic 3D vortex sheet, using (1.3).

We let $P(\varphi) = \delta(\varphi)$ (in practice δ is replaced by an approximation). The zero level set of φ is the vortex sheet $\Gamma(s)$, parameterized by surface area s. The variable η_0 is chosen to fit the initial vortex sheet strength. For instance, given any smooth test function g

$$\begin{aligned} \langle \xi, g \rangle &= \langle \eta_0 \delta(\varphi_0), g \rangle \\ &= \int \eta_0(\Gamma_0(s)) g(\Gamma_0(s)) \frac{1}{|\nabla \varphi_0|} ds \end{aligned}$$

Thus, the initial vortex sheet strength is given by

$$\frac{\eta_0}{|\nabla \varphi_0|} \tag{3.1}$$

To obtain the velocity vector, one introduces the vector potential A, where

$$v = \nabla \times A, \quad div(A) = 0$$

and solves the Poisson equation

$$\triangle A = -P(\varphi)\eta \tag{3.2}$$

To ensure that $div(A) = 0$, we require that $div(\eta) = 0$ and that $\nabla\varphi \cdot \eta = 0$ initially. It is easy to see that these equalities are maintained as t increases.

The boundary conditions for the velocity are $v_2(x, \pm 1, z) = 0$ and periodic in x and z. To obtain the boundary conditions for $A = (A_1, A_2, A_3)$, we use the divergence free condition on A in addition to the velocity boundary condition. Thus,

$$\begin{aligned} A_1(x, \pm 1, z) = A_3(x, \pm 1, z) &= 0 \\ \partial_y A_2(x, \pm 1, z) &= 0 \end{aligned} \tag{3.3}$$

and periodic in x, z. The Neumann condition requires the following compatibility condition

$$\int \xi_2(x, y, z, 0) dx dy dz = 0$$

Three dimensional runs are much more expensive than two dimensional runs, not only because the number of grid points increases, but also because there are now four evolution equations (for φ and η), and three potential equations. We still use the third order ENO scheme coupled with the second order elliptic solver FISHPAK, with 64^3 grid points, and ϵ is chosen as $6\Delta x$, which is the same in magnitude as that used in Figure 1 of Example 2.1. The boundary conditions for φ are similar to the ones in two dimensions: periodic in all directions (module the linear term in y). The vortex sheet strength vector η is periodic in all directions.

We first verify whether we can recover the two dimensional results with the three dimensional setting. We use the initial condition

$$\varphi_0(x, y, z) = y + 0.05 \sin(\pi x)$$

which is the same as that for Example 2.1, and choose a constant initial condition for η as $\eta_0(x, y, z) = (0, 0, 1)$. We observe exact agreement with our two dimensional results in Example 2.1, Figure 1.

Next, we consider the truly three dimensional problem with the initial condition chosen as

$$\varphi_0(x, y, z) = y + 0.05 \sin(\pi x) + 0.1 \sin(\pi z)$$

and η is chosen as $\eta_0(x, y, z) = (0, -0.1\pi \cos(\pi z), 1)$ which satisfies the divergence free condition as well as the condition to be orthogonal to $\nabla\varphi$. In Figures 7(a) to 7(f), we show the level set of $\varphi = 0$ for $t = 0$, 1, 2, 3, 4 and 5. We can clearly see the roll up process and the three dimensional features as time increases. The cuts at the constants $z = 0$ and $x = 0$ planes are shown in Figures 8 and 9.

Example 2 - Vortex Filaments. In this example, P is an approximate delta function P_ϵ, where ϵ is the filament core size. The level set function φ is supported on a curve γ, which is the filament centerline. For example, initially, φ_0 may be chosen to be the distance function to γ_0. The vorticity strength η_0 is chosen to fit the initial filament strength.

It is known that the velocity of the filament is given asymptotically by $\kappa log(\frac{1}{\epsilon})$ (κ is the curvature of γ) [10].

A possible set of boundary conditions corresponds to zero normal velocity everywhere, i.e. $v_1(\pm 1, y, z) = 0$, $v_2(x, \pm 1, z) = 0$, $v_3(x, y, \pm 1) = 0$. The corresponding boundary conditions on the vector potential A are similar to (3.3).

4 Conclusions

We introduce a new formulation for the Euler Equations that allows the computation of flows with highly concentrated vorticity using an Eulerian grid. Traditionally, such flows have been computed in Lagrangian coordinates. This formulation is very simple and very easy to implement in practice, and has the advantage of handling topological singularities automatically. In addition, no explicit filtering is necessary, in order to handle the ill-posedness of the underlying interface problem. Our calculation of a three dimensional vortex sheet seems to be the first successful Eulerian calculation in which the surface feeds back into the calculation of the velocity of the flow. Vortex in cell calculations for three dimensional vortex sheets were done earlier by Trygvasson et al in [16].

In future work, we shall explore more efficient algorithms using adaptive mesh refinement techniques.

Acknowledgment

The authors would like to thank R. Caflisch, B. Engquist, R. Krasny, B. Merriman and P. Smereka for helpful discussions related to this work. The computation reported in this paper is supported by the Pittsburgh Supercomputer Center.

References

[1] A. Bertozzi and P. Constantin, *Global regularization for vortex patches*, Commun. Math. Phys., v152, 1993, pp.19-28.

[2] G. R. Baker and M. J. Shelley, *On the connection between thin vortex layers and vortex sheets*, J. Fluid Mech., v215, 1990, pp.161-194.

[3] J.-Y. Chemin, *Persistance de structures geometriques dans les fluides incompressibles bidimensionels*, preprint 1991, Annales de l'Ecole Normale Superieure, v26, 1993, pp.1-26.

[4] W. E and C.-W. Shu, *A numerical resolution study of high order essentially non-oscillatory schemes applied to incompressible flow*, J. Comput. Phys., v110, 1994, pp.39-46.

[5] E. Harabetian and S. Osher, *Regularization of ill-posed problems via the level set approach*, UCLA CAM Report 95-41 (1995), submitted to SIAM J. Appl. Math (1995).

[6] R. Krasny, *A study of singularity formation in a vortex sheet by the point-vortex approximation*, J. Fluid Mech., v167, 1986, pp.65-93.

[7] R. Krasny, *Desingularization of periodic vortex sheet roll-up*, J. Comput. Phys., v65, 1986, pp.292-313.

[8] R. Krasny, *Vortex sheet computations: roll-up, wakes, separation*, in *Proc. AMS-SIAM Summer Seminar in Applied Math, "Vortex Methods and Vortex Dynamics"*, C. Anderson and C. Greengard, Editors, 1991.

[9] R. Krasny, *A vortex dipole sheet model for a wake*, Phys. Fluids A, v1, 1989, pp.173-175.

[10] H. Lamb, Hydrodynamics, Dover, New York, 1945.

[11] S. Osher, *Subscale capturing in numerical analysis*, in *Proceedings of ICM*, Zurich, 1994 (to appear).

[12] S. Osher and J.A. Sethian, *Fronts propagation with curvature dependent speed, algorithms based on a Hamilton-Jacobi formulation*, J. Comput. Phys., v79, 1988, pp.12-49.

[13] S. Osher and C.-W. Shu, *High-order essentially nonoscillatory schemes for Hamilton-Jacobi equations*, SIAM J. Num. Anal., v28, 1991, pp.907-922.

[14] C.S. Peskin, *Numerical analysis of blood flow in the heart*, J. Comput. Phys., v25, 1977, pp.220-252.

[15] M. Sussman, P. Smereka, S. Osher, *A level set approach for computing solutions to incompressible two phase flow*, J. Comput. Phys., v114, 1994, pp.146-159.

[16] G. Trygvasson, W.J.A. Dahm, K. Sbeih, *Fine structure of vortex sheet rollup by viscous and inviscid simulation*, J. Fluids Engin., v113, 1991, pp.31-36.

[17] N. Zabusky, M.H. Hughes, and K.V. Roberts, *Contour dynamics for the Euler equations in two dimensions*, J. Comput. Phys., v30, 1979, pp.96-106.

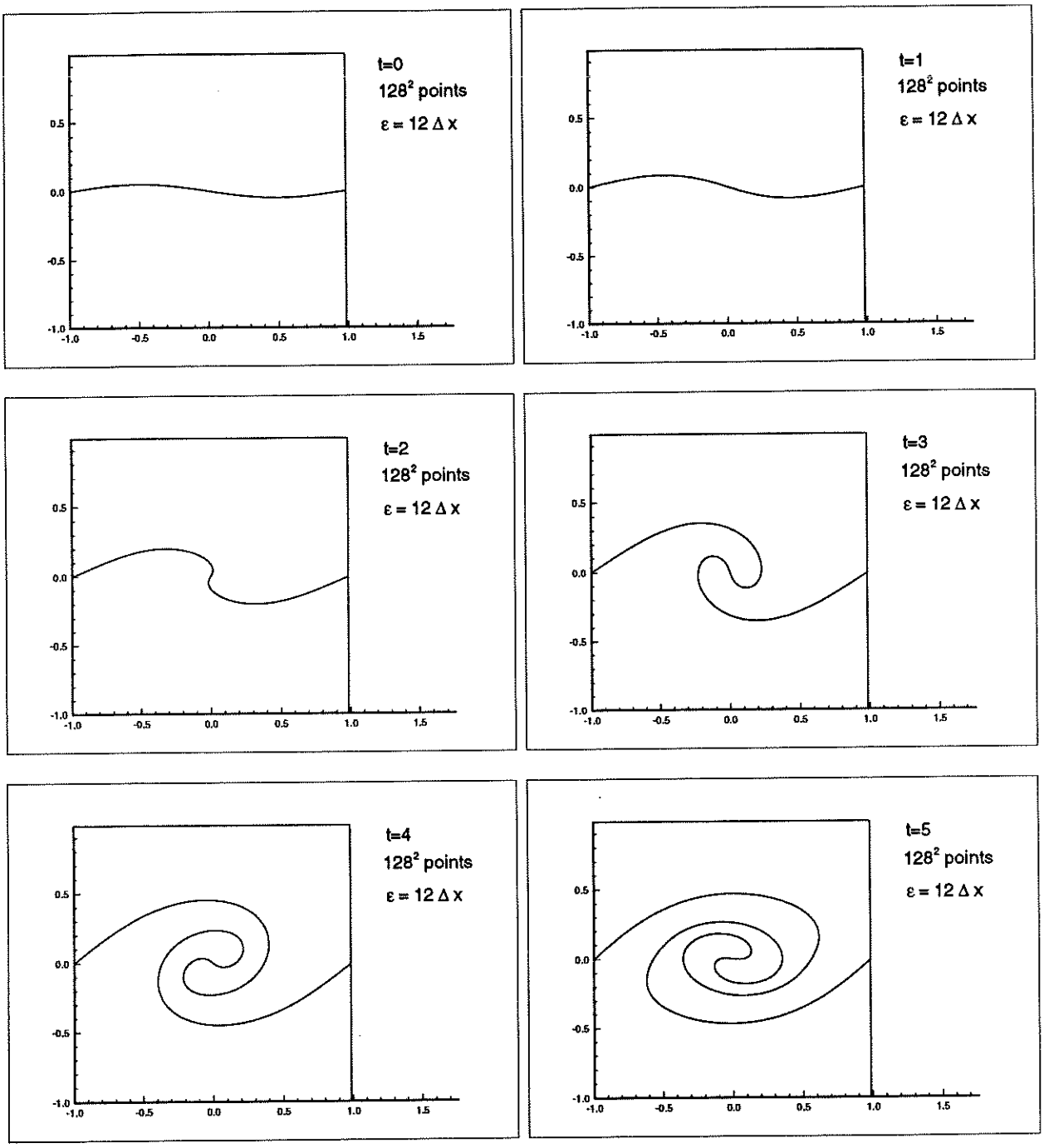

Figure 1: Two dimensional vortex sheet simulation. 128^2 grid points. $\epsilon = 12\Delta x$. 1(a) (top, left): t=0; 1(b) (top, right): t=1; 1(c) (middle, left): t=2; 1(d) (middle, right): t=3; 1(e) (bottom, left): t=4; 1(f) (bottom, right): t=5.

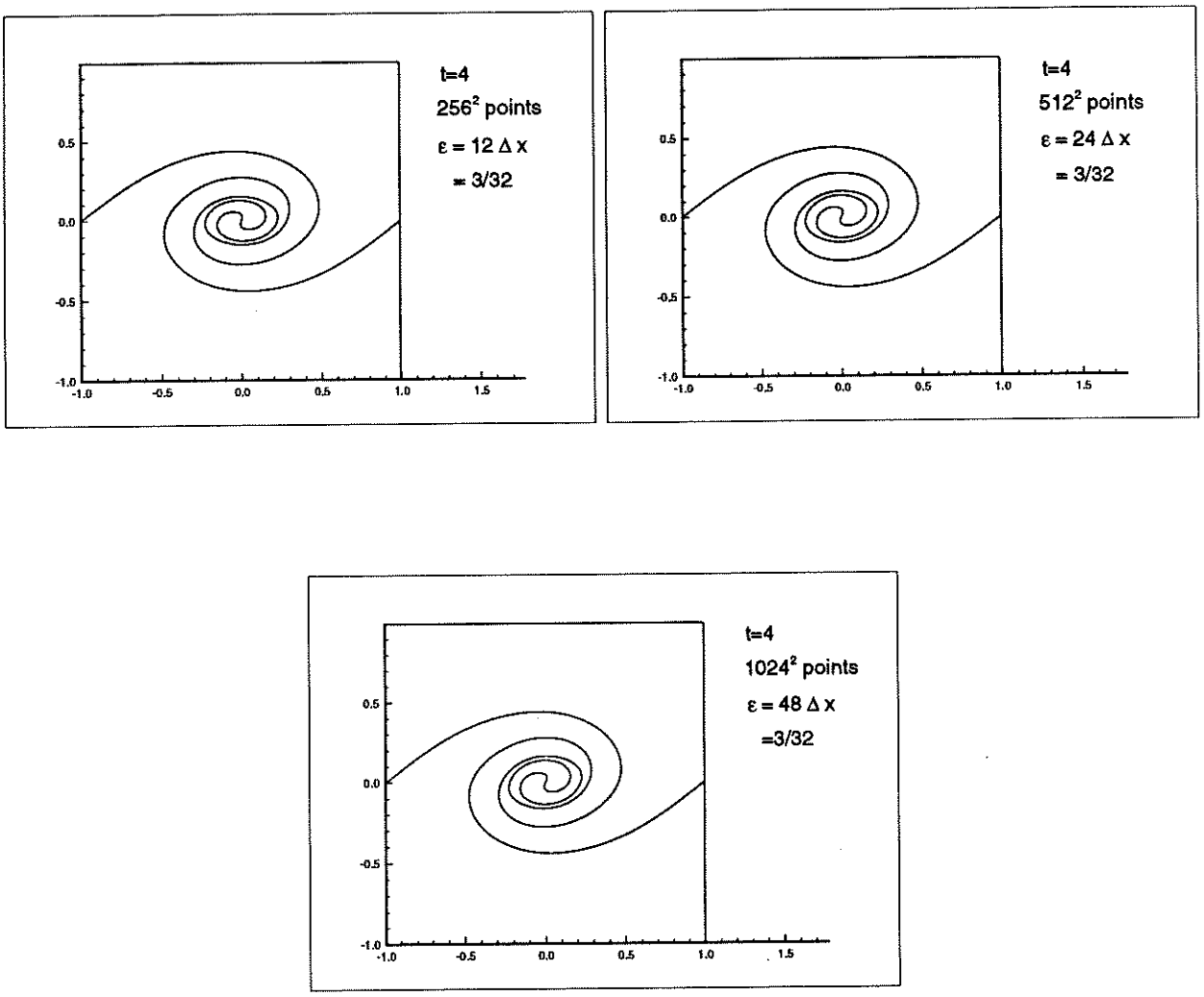

Figure 2: Two dimensional vortex sheet simulation. Fixed δ function width $\epsilon = \frac{3}{32}$, at t=4. 2(a) (top, left): 256^2 points; 2(b) (top, right): 512^2 points; 2(c) (bottom): 1024^2 points.

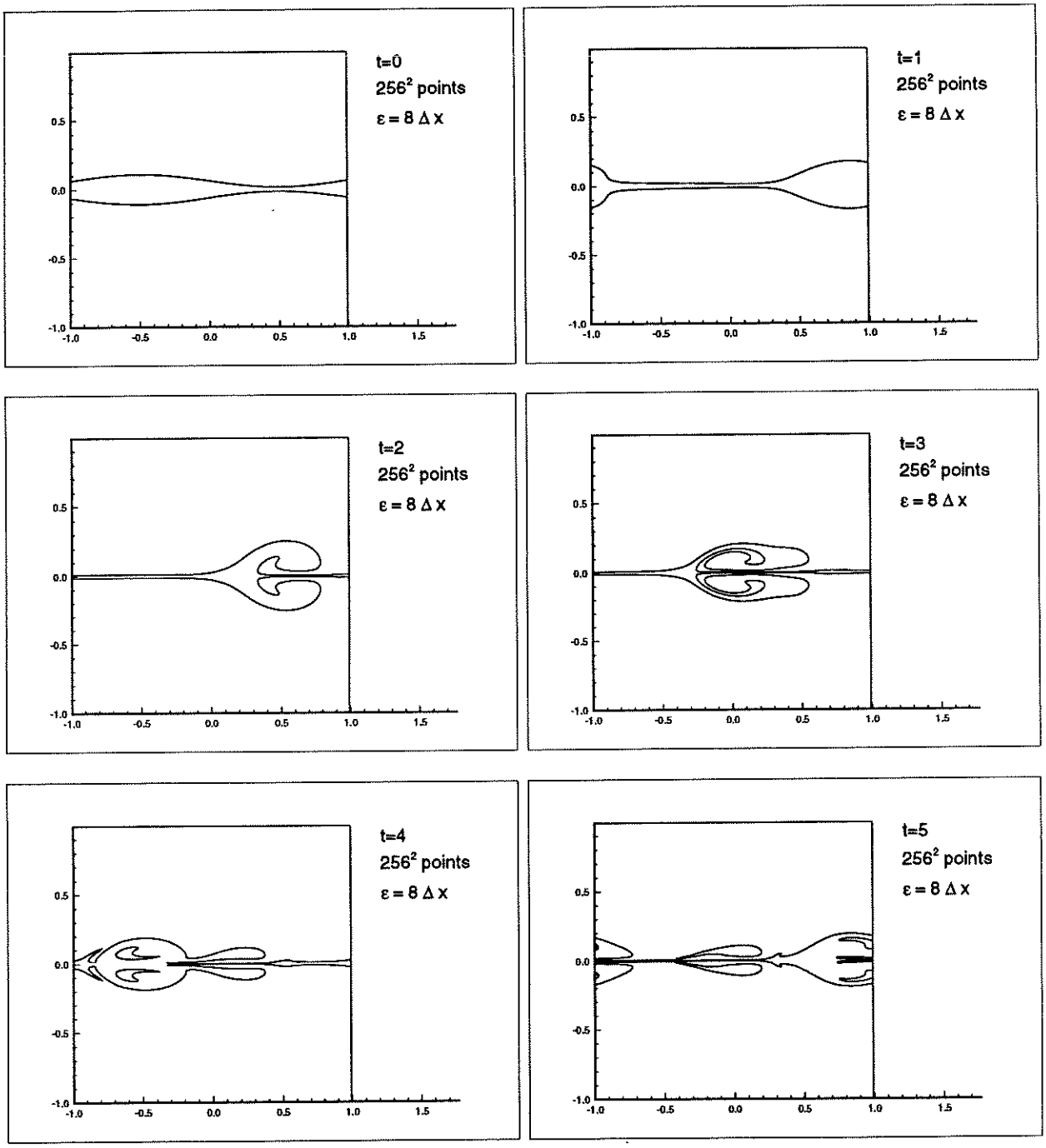

Figure 3: Two dimensional vortex sheet dipole simulation. 256^2 grid points. $\epsilon = 8\Delta x$. 3(a) (top, left): t=0; 3(b) (top, right): t=1; 3(c) (middle, left): t=2; 3(d) (middle, right): t=3; 3(e) (bottom, left): t=4; 3(f) (bottom, right): t=5.

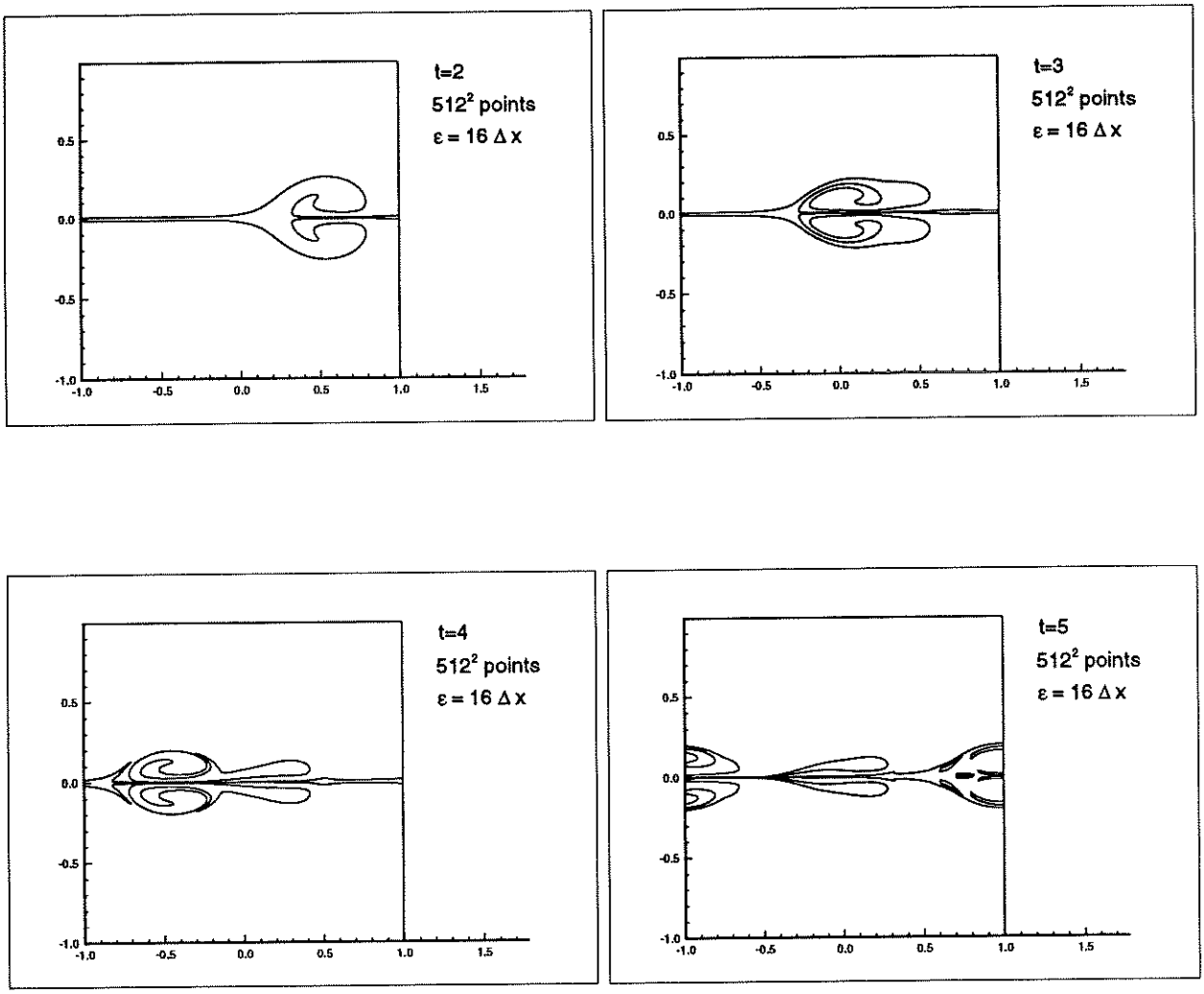

Figure 4: Two dimensional vortex sheet dipole simulation. 512^2 grid points. $\epsilon = 16\Delta x$. 4(a) (top, left): t=2; 4(b) (top, right): t=3; 4(c) (bottom, left): t=4; 4(d) (bottom, right): t=5.

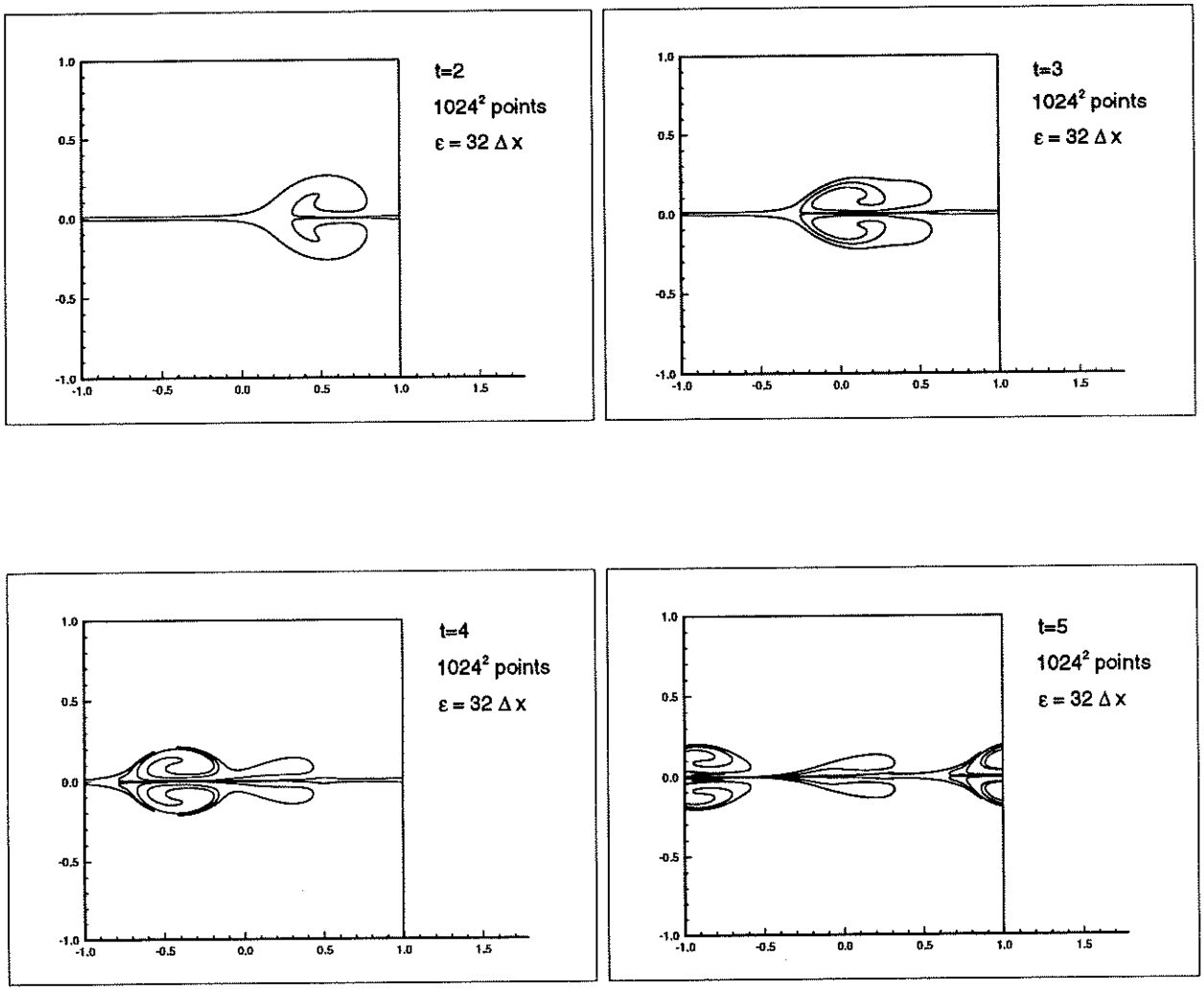

Figure 5: Two dimensional vortex sheet dipole simulation. 1024^2 grid points. $\epsilon = 32\Delta x$. 5(a) (top, left): t=2; 5(b) (top, right): t=3; 5(c) (bottom, left): t=4; 5(d) (bottom, right): t=5.

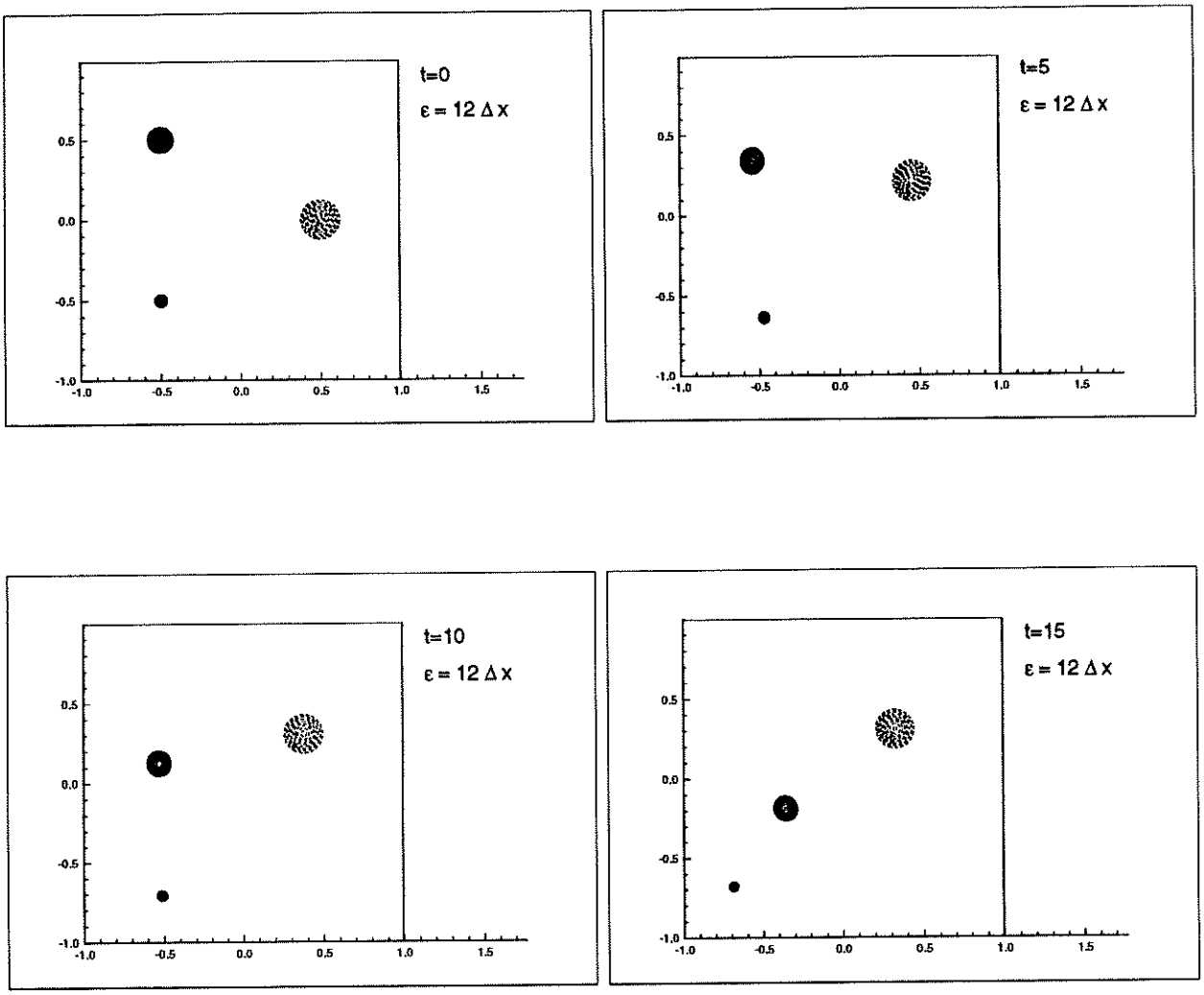

Figure 6: Two dimensional point vortices simulation. 256^2 grid points. $\epsilon = 12\Delta x$. 10 contour lines between $\varphi = 0$ and $\varphi = 0.04$. Solid lines for φ_+ and dashed lines for φ_-. 6(a) (top, left): t=0; 6(b) (top, right): t=5; 6(c) (bottom, left): t=10; 6(d) (bottom, right): t=15.

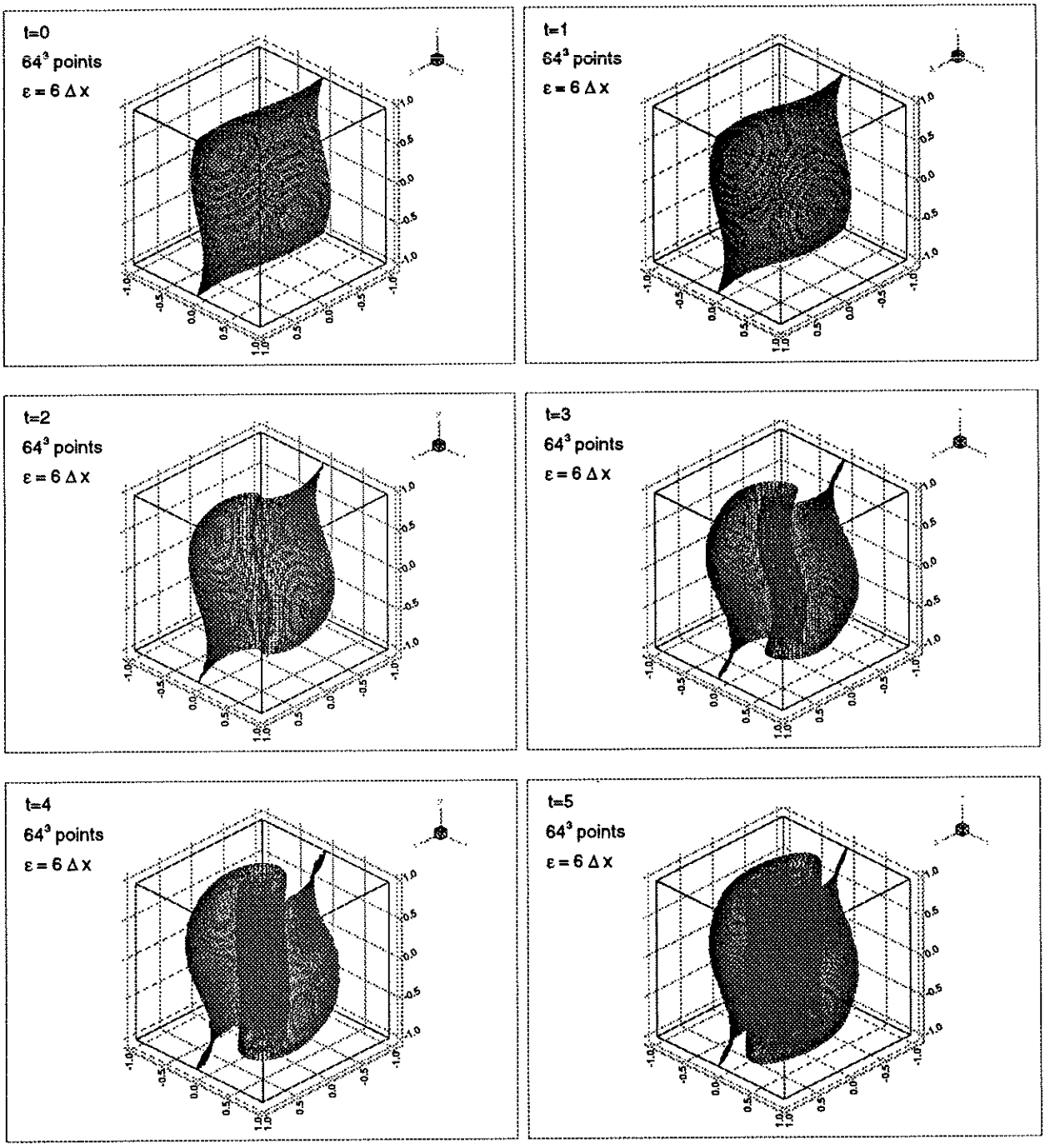

Figure 7: Three dimensional vortex sheet simulation. 64^3 grid points. $\epsilon = 6\Delta x$. 7(a) (top, left): t=0; 7(b) (top, right): t=1; 7(c) (middle, left): t=2; 7(d) (middle, right): t=3; 7(e) (bottom, left): t=4; 7(f) (bottom, right): t=5.

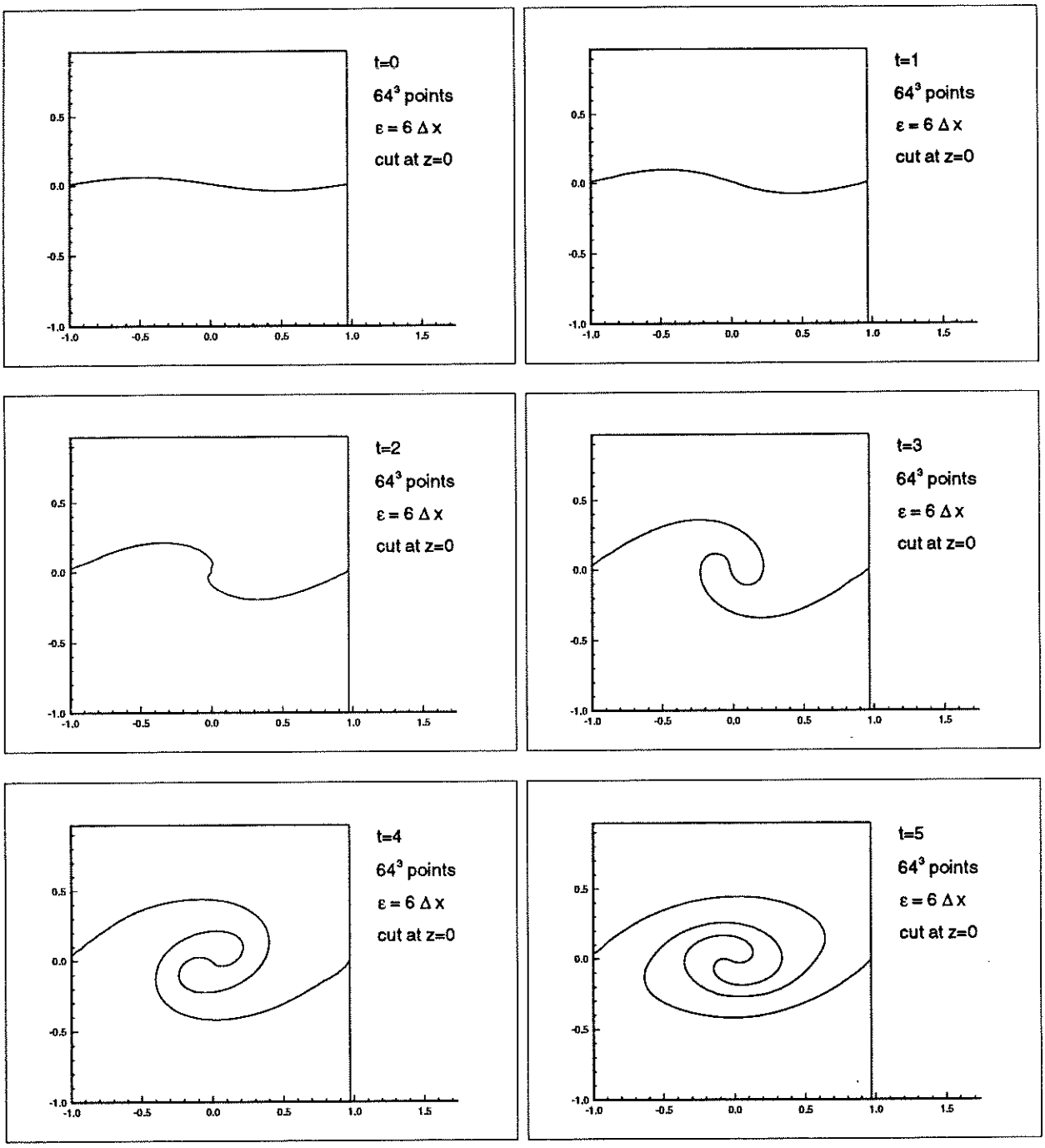

Figure 8: The $z = 0$ plane cut for the three dimensional vortex sheet simulation. 64^3 grid points. $\epsilon = 6\Delta x$. 8(a) (top, left): t=0; 8(b) (top, right): t=1; 8(c) (middle, left): t=2; 8(d) (middle, right): t=3; 8(e) (bottom, left): t=4; 8(f) (bottom, right): t=5.

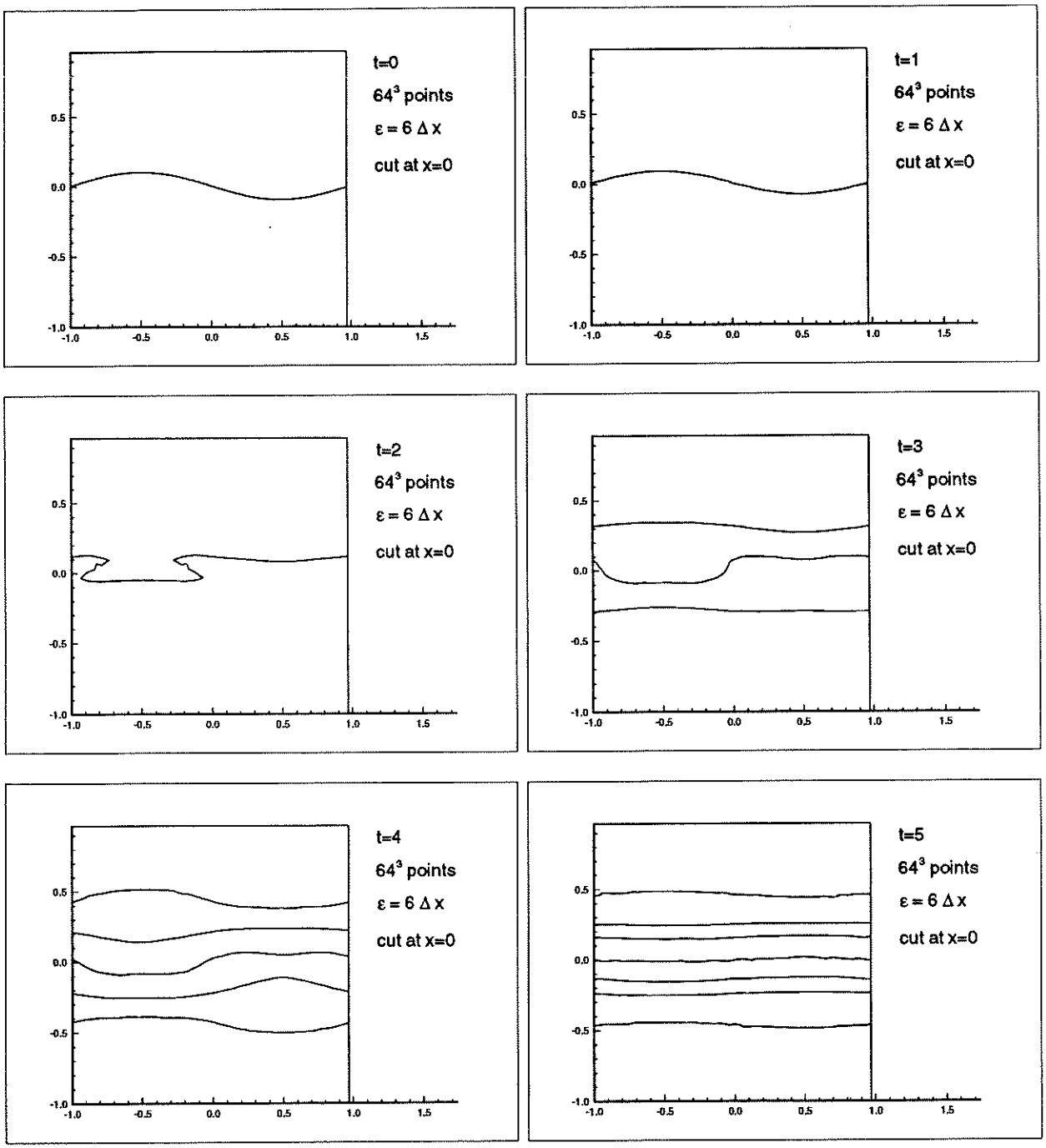

Figure 9: The $x = 0$ plane cut for the three dimensional vortex sheet simulation. 64^3 grid points. $\epsilon = 6\Delta x$. 9(a) (top, left): t=0; 9(b) (top, right): t=1; 9(c) (middle, left): t=2; 9(d) (middle, right): t=3; 9(e) (bottom, left): t=4; 9(f) (bottom, right): t=5.